

Asteroid detection at millimetric wavelengths

with the PLANCK survey

G. Cremonese^a, F. Marzari^b, C. Burigana^c, M. Maris^d

^a*INAF-Osservatorio Astronomico, Vicolo Osservatorio 5, I-35122, Padova, Italy*

^b*Dipartimento di Fisica, Università di Padova, Via Marzolo 8, I-35131, Padova, Italy*

^c*Istituto TeSRE, Consiglio Nazionale delle Ricerche, Via Gobetti 101, I-40129, Bologna, Italy*

^d*INAF-Osservatorio Astronomico, Via G.B. Tiepolo 11, I-34131, Trieste, Italy*

¹ The address to which the proofs have to be sent is:

Gabriele Cremonese, Osservatorio Astronomico, Vicolo Osservatorio 5, I-35122, Padova, Italy

fax: +39-049-8759840

e-mail: cremonese@pd.astro.it

Abstract

The PLANCK mission, originally devised for cosmological studies, offers the opportunity to observe Solar System objects at millimetric and submillimetric wavelengths. We concentrate in this paper on the asteroids of the Main Belt, a large class of minor bodies in the Solar System. At present more than 40000 of these asteroids have been discovered and their detection rate is rapidly increasing. We intend to estimate the number of asteroids that can be detected during the mission and to evaluate the strength of their signal. We have rescaled the instrument sensitivities, calculated by the LFI and HFI teams for sources fixed in the sky, introducing some degradation factors to properly account for moving objects. In this way a detection threshold is derived for asteroidal detection that is related to the diameter of the asteroid and its geocentric distance. We have developed a numerical code that models the detection of asteroids in the LFI and HFI channels during the mission. This code performs a detailed integration of the orbits of the asteroids in the timespan of the mission and identifies those bodies that fall in the beams of Planck and their signal strength. According to our simulations, a total of 397 objects will be observed by PLANCK and an asteroidal body will be detected in some beam in 30% of the total sky scan-circles. A significant fraction (in the range from ~ 50 to 100 objects) of the 397 asteroids will be observed with a high S/N ratio.

Flux measurements of a large sample of asteroids in the submillimeter and millimeter range are relevant since they allow to analyze the thermal emission and its relation to the surface and regolith properties. Furthermore, it will be possible to

check on a wider base the two standard thermal models, based on a nonrotating or rapidly rotating sphere.

Our method can also be used to separate Solar System sources from cosmological sources in the survey. This work is based on PLANCK LFI activities.

Key words: Astronomical and space-research instrumentation, Astronomical observations: Radio, microwave, and submillimeter, Solar System: Asteroids

PACS: 95.55.n, 95.85.Bh, 96.30.Ys

1 Introduction

The PLANCK ESA mission² will perform a high-angular resolution mapping of the microwave sky over a wide range of frequencies, from 30 to 900 GHz. These data will have important implications on different fields, from cosmology and fundamental physics to Galactic and extragalactic astrophysics. The Solar System astronomy will also benefit from the Planck mission since it will offer the opportunity to perform a survey of Solar System objects at millimetric wavelengths. Planck will be sensitive to the millimetric emissions from planets and from a significant fraction of the asteroidal population. In this paper we focus on the detection of asteroid radio emissions and on the identification of the asteroidal targets that will be observed during the mission. The relevant parameters for the possible detection of a minor body by PLANCK are the geocentric distance and the diameter. We will concentrate in this paper on Main Belt asteroids that can be more easily detected since their orbits are at relatively small geocentric distances and several objects have diameter larger than 50 km.

Radio observations of asteroids from the Earth were performed by Redman et al. (1998) at seven different frequencies ranging from 150 to 870 GHz. Redman focused on the information that radio data can give to the thermal models of asteroids. Their set of targets included 5 asteroids already observed by Altenhoff et al. (1994) and two new objects. Altenhoff et al. (1994) observed, at

² <http://astro.estec.esa.nl/SA-general/Projects/Planck/>

250 GHz, 15 among the largest asteroids, but only to determine the diameter and to compare their measurements with other methods.

The emissivity obtained at radio frequencies may probe the temperature of the body at different depths on the surface allowing to derive precise values of the average temperature. Moreover, relevant physical data concerning the density of the regolith layer covering the surface of the asteroids can also be determined.

Radio observations of asteroids by PLANCK offer a unique opportunity to improve our knowledge on the thermal emission in the millimetric and sub-millimetric domain, increasing our knowledge of the physical nature of the surface layers of the objects. Considering that radio data provide an estimate of the density on a scale related to the wavelength of the observations, the advantage of using Planck will be in the possibility of gathering data on a large frequency spectrum and then to probe the temperature and regolith density at different depths below the surface.

Furthermore, the PLANCK data can help to refine the thermophysical models using also physical studies of the thermal properties of stony and FeNi meteorites as well as inferences about surface physical properties derived from asteroid radar studies. It will be possible to relate the PLANCK data to the two standard models which are commonly invoked to predict the thermal radiation from asteroids, considering the asteroid as a nonrotating sphere or a rapidly rotating sphere.

For instance Vesta has been observed on a wide range of wavelengths, from

submillimeter to centimeter, and the ratio of the observed flux, at each wavelength (from $12\mu\text{m}$ to 6cm), divided by the flux expected from a blackbody at the temperature of a nonrotating asteroid shows a behavior different from the standard models (Redman et al. 1992). A successful model for the thermal emission must explain why the apparent flux remains below the rapidly rotating sphere value, and much below the nonrotating sphere value, over the entire submillimeter range. Several mechanisms can lower the apparent temperature at radio wavelengths as reflections at the outer surface of the regolith, reduction in the actual temperature of the deeper layers of the regolith due to diurnal temperature variations at the surface, or scattering by grains within the regolith which can reduce the emissivity in a wavelength dependent fashion. The actual emission from an asteroid may combine all three effects in differing amounts at each wavelength, but only very few objects have been observed in the submillimeter and millimeter range and it is not possible to identify a typical behavior or to relate the results to different asteroid taxonomic classes.

It is worth to point out that the main belt asteroids may represent a source of background for the PLANCK mission and, as a consequence, they should be considered in the definition of the scientific and technical aspects of the mission.

The thermal emission of asteroids, apart from their intrinsic scientific relevance, has also to be considered as a potential source of spurious detections in the analysis of Galactic or extragalactic sources. The precise determination

at each epoch of the eventual presence of an asteroid, with its point emission, in some of the PLANCK beams is a critical requirement to avoid systematic errors in mapping the astrophysical sources of radiation. The high nominal accuracy of the PLANCK instruments suggests a tight control even for the contamination from asteroids below the detection threshold.

Section 2 is devoted to the discussion of the PLANCK sensitivity for the detection of moving sources at different frequency channels. The averaged final PLANCK sensitivities will be rescaled in order to take into account the positions of the different antenna beams in the telescope field of view and the main properties of the PLANCK scanning strategy. These results are used in Section 3 to determine the threshold to detect asteroids in the PLANCK data streams, according to their typical temperature and size. In Section 4, we describe our numerical code to compute the asteroid transits on the different PLANCK beams and to estimate their signals. The results of this analysis are presented in Section 5. Finally, we discuss the results and draw our main conclusions in Section 6.

2 PLANCK performances

The PLANCK surveyor will observe the sky at nine frequencies with two instruments having different angular resolutions and sensitivities: the Low Frequency Instrument (LFI) that covers the range 30-100 GHz, and the High Frequency

Table 1

Instrumental performances and confusion noise estimates for PLANCK LFI. The bandwidths are 20% for the LFI channels and 25% for the HFI ones.

ν_{eff} (GHz)	$N_{\text{rad;bol}}$ (unpol;pol)	FWHM (arcmin)	σ_{noise} (μK)	σ_{noise} (mJy)	σ_{CMB} (mJy)	$\sigma_{\text{ex.sou.}}$ (mJy)	σ_{Gal} (mJy)	$\sigma_{\text{noise,MAP}}$ (mJy)
30	4	33.6	5.1	13.4	245	60	100	48
44	6	22.9	7.8	20.5	238	45	45	69
70	12	14.4	10.6	28.0	221	30	15	102
100	32	10.0	12.8	33.2	192	20	7	127
100	4 ; 0	10.7	2.9	8.7	192	20	7	127
143	3 ; 9	8.0	3.4	11.5	149	15	6	–
217	4 ; 8	5.5	3.1	11.5	82.6	8–15	5	–
353	6 ; 0	5.0	2.4	19.4	19.1	20–35	18	–
545	0 ; 8	5.0	2.0	38	1.5	45–80	62	–
857	6 ; 0	5.0	0.9	43	0.016	100–180	120	–

Instrument (HFI) that covers the range 143–857 GHz. In Table 1 we report the relevant parameters for both LFI and HFI (see columns 1, 4 and 5). The relative bandwidths of the LFI and HFI are respectively $\simeq 20\%$ and $\simeq 25\%$ (see column 2 of Table 1).

In this work we will refer to the nominal PLANCK sensitivity per resolution

element (a squared pixel with side equal to the Full Width at Half Maximum (FWHM) of the corresponding beam), as recently revised by the LFI Consortium (PLANCK Low Frequency Instrument, Instrument Science Verification Review, October 1999, LFI Design Report, private reference; see also the LFI proposal, Mandolesi et al. (1998)) and as reported in the HFI proposal (Puget et al. 1998). The sensitivity is related to the measurement of microwave anisotropy in terms of antenna temperature and flux

The normalized sensitivity per pixel in the sky (i.e., the sensitivity divided by the averaged sensitivity of the observed pixels in the sky) for a typical PLANCK beam improves with the module of the ecliptic latitude up to a ring of optimal sensitivity which contains a small unobserved sky region. The normalized sensitivity averaged over the ecliptic longitudes as a function of the ecliptic colatitude is close to unit at the ecliptic colatitude $\theta_e \simeq 50^\circ$ and 130° and it is quite well approximated by the law $\sqrt{\sin \theta_e / \sin 50^\circ}$ at least for ecliptic latitudes between about -70° and $+70^\circ$, relevant for Solar System objects. The detailed behavior of the sensitivity on θ_e is clearly dependent on the choice of the scan angle α , the adopted scanning strategy and the beam position on the telescope field of view.

The Solar System bodies are moving objects and most likely they have a variable flux depending from their heliocentric and geocentric distances. It means that their observation and estimate of their fluxes can not take easily advantage from the twice coverage of the sky, during the planned period of observation of 14 months, nor from the coadding of data from different feeds

if they look at different sky positions at the same time. Further details on the PLANCK sensitivity relevant for moving bodies and variable sources can be found in (Burigana 2000) and (Burigana 2001). For the LFI sensitivities we take into account the most recent computations of the LFI beam positions of the telescope field of view (Sandri & Villa 2001). The HFI channels can play a crucial role for the study of the moving bodies of the Solar System, as their spectra are typically close to blackbodies, or modified blackbodies, at temperatures significantly higher than the cosmic microwave background (CMB) or are dominated by dust emission components or by molecular emission lines, particularly relevant at the highest PLANCK frequencies (see, e.g., Neufeld et al. (2000)).

The PLANCK receivers are affected by the $1/f^\alpha$ (with α in the range from ~ 1 to ~ 2) noise that introduces drifts in the time ordered data identified as stripes in the final maps (Janssen et al. 1996). The time ordered data have to be cleaned from these drifts by using appropriate data reduction methods. Destriping algorithms (see, e.g., Delabrouille (1998), Maino et al. (2001), and references therein) are able to efficiently remove $1/f^\alpha$ noise drifts by working directly in the time domain, fully preserving the time ordering of the data and allowing to exploit the cleaned data to properly reveal the signatures from moving and variable sources. Then it is possible to neglect the drift contamination in the following discussion. We note also that destriping algorithms (as well as other classes of reduction methods) use the comparison between repeated observations at different times of the same sky positions to remove

drifts. Therefore, cleaning the time ordered data from astrophysical moving or variable sources by properly flagging the time ordered data may be useful to improve the destriping codes, according to the S/N ratios of the contaminating sources (the possibility to use flagged data have been already implemented in the most recent version of the LFI destriping code, see Stanghellini et al. (2001)). Running this task represents a minor effort for the data reduction pipeline and it can be implemented starting from the software developed with this work.

In addition to the instrumental noise, the sky itself introduces a confusion noise given by the Galactic and extragalactic temperature fluctuations and from the CMB anisotropies, relevant at different angular scales, $\theta \simeq 180^\circ/\ell$, where ℓ is the multipole of the harmonic expansion of the temperature fluctuation pattern. We report in Table 1 the fluctuation level of the CMB anisotropy assuming a rms thermodynamic temperature fluctuation of about $95 \mu\text{K}$ as derived for a standard cosmological flat model, approximately COBE/DMR normalized with cosmological parameters compatible with the present constraints on CMB fluctuations at moderate multipoles, as derived from recent balloon experiments. Of course, the accurate determination of the CMB confusion noise at small scales is the PLANCK main goal.

Then we report the extragalactic source confusion noise (by taking into account both radio and infrared sources), as evaluated by Toffolatti et al. (1998) and revised by De Zotti et al. (1999a) and De Zotti et al. (1999b). We estimate a more precise source confusion noise as $\sigma_{ex.sou.} = \sqrt{C_l}/(\text{FWHM}/\text{rad})$ where

the angular power spectrum C_l is the sum of the C_l of radio and far-IR source fluctuations, as quoted by De Zotti et al. (1999b) for a conservative detection limit of 1 Jy (see their Table 6). These estimates may be then pessimistic. On the other hand, it would be probably difficult to subtract sources in real time with high accuracy; in addition, the source clustering, neglected in this work, may significantly increase the source confusion noise, at least for some cosmological models, particularly at the highest PLANCK frequencies (Magliocchetti et al. 2001).

The Galactic fluctuation levels reported here are only indicative and refer to moderate and high Galactic latitudes, as large variations are present in the sky.

The relevant global sensitivity for point source detection/observation is typically assumed to be the sum in quadrature of all the sources of confusion noise, multiplied by a proper constant (typically in the range from ~ 2 to 5). We report also in the last column of Table 1 the sensitivity of the MAP experiment³ ($\sim 35\mu\text{K}$, in terms of thermodynamic temperature, on squared pixels with 0.3° side at each frequency channel, 22, 30, 40, 60 and 90 GHz), rescaled at the corresponding PLANCK beam size. In fact, we can argue that after the MAP mission the sum of the CMB and foreground temperature fluctuations on each sky pixel will be known with the MAP accuracy. CMB anisotropy experiments provide time ordered data and then maps of

³ <http://map.gsfc.nasa.gov/html/>

temperature fluctuations, δT , from the average temperature; the temperature fluctuations can be expressed in terms of fluctuations of antenna temperature, δT_{ant} , or in terms of fluctuations of thermodynamic temperature, δT_{therm} . Their ratio is given by:

$$\frac{\delta T_{ant}}{\delta T_{therm}} = \frac{x^2 \exp(x)}{[\exp(x) - 1]^2}, \quad (1)$$

where $x = h\nu/kT_0$, $T_0 \simeq 2.725$ K being the CMB monopole thermodynamic temperature as established by Mather et al. (1999). The same formula holds for ratio between the rms noise of the observed antenna temperature fluctuation, $\Delta\delta T_{ant}$, and the rms noise of the observed thermodynamic temperature fluctuation, $\Delta\delta T_{therm}$.

In the study of discrete sources it is preferable to express the signal fluctuations in terms of flux fluctuations. For a point source with flux F_ν observed with a beam response J normalized to the beam maximum response, the observed antenna temperature is given in general by:

$$T_{\nu,ant,obs} = 10^{-41} (c^2/2k) [(F_\nu/\text{Jy})/(\nu/\text{GHz})^2] (J / \int_{4\pi} J d\Omega). \quad (2)$$

Assuming a beam quite well approximated by a Gaussian shape, as in the case of PLANCK beams, the integral of the antenna pattern is given by $\int_{4\pi} J d\Omega \simeq (\pi/4\ln 2)(\text{FWHM}/\text{rad})^2$. In this work we deal with sources with weak or moderate flux, i.e. essentially detectable only when they fall within a pixel with a side $\sim \text{FWHM}$ about the beam center. For a first order evaluation of the source

flux sensitivity estimate we can then neglect the information contained in the time ordered data outside the pixel with a side $\sim \text{FWHM}$ about the beam center, assume the PLANCK sensitivity per pixel of side $\sim \text{FWHM}$, and approximate the beam response as unit within a pixel with a side $\simeq \text{FWHM}$ about the beam center and null outside in the relationship between the antenna temperature and the flux reported in the following, i.e. $J / \int_{4\pi} J d\Omega \simeq 1/(\text{FWHM}/\text{rad})^2$ within a pixel with a side $\simeq \text{FWHM}$ about the beam center and $J / \int_{4\pi} J d\Omega = 0$ outside.

In this approximation, the relationship between the flux fluctuation and the antenna temperature fluctuation induced by a discrete source on a squared pixel with side $\Delta\theta$ ($\simeq \text{FWHM}$) is:

$$\frac{\delta B_\nu/\text{Jy}}{[\delta T_{ant}/\text{mK}]} \simeq 30.7[\nu/\text{GHz}]^2[\Delta\theta/\text{rad}]^2, \quad (3)$$

and the same formula holds for ratio between the rms noise of the observed flux fluctuation, $\Delta\delta B_\nu$, and the rms noise of the observed antenna temperature fluctuation, $\Delta\delta T_{ant}$, on a pixel of side $\simeq \text{FWHM}$. This approximation is used to translate the HFI sensitivities quoted by Puget et al. (1998) in terms of total flux fluctuation to the antenna temperature fluctuation sensitivities reported in Table 1. More detailed analyses, able to take into account the complexity of beam shapes, the pointing uncertainty and other relevant systematical effects will be considered in future technical works and included in the data analysis pipeline.

We will derive the PLANCK sensitivity at the different channels, relevant for the study of moving objects from the PLANCK time ordered data, by rescaling the sensitivities of the final PLANCK maps. At $\nu \lesssim 100$ GHz it would be possible to exploit the microwave maps derived from MAP data and cleaned at the level of MAP sensitivity from the effect of source flux variations and moving objects. In this case the 1σ sensitivity levels, relevant for the following discussions considering the MAP data, will be the sum in quadrature of the PLANCK sensitivities, appropriately rescaled, and of the sensitivities of the final MAP data. These values will be also the sensitivities to be used to detect and to study the moving objects before producing the PLANCK maps. On the other hand, after the PLANCK data analysis and the production of the PLANCK cleaned maps at all frequencies, we may be able to take advantage from the knowledge of the sky fluctuation in the positions of the considered moving objects. The sensitivity will be close to the final one of the PLANCK maps multiplied by $\sqrt{2}$, i.e. about a factor 2 better than the MAP final sensitivity in the common frequency range, because a moving object will not have the same position in the following PLANCK sky coverage.

2.1 PLANCK sensitivity for moving sources

The PLANCK sensitivity relevant for the study of moving sources has to be properly rescaled with respect to that reported in Table 1 to include several

factors of sensitivity degradation.

A first sensitivity degradation factor, $\sim \sqrt{2}$, derives by considering only a single sky coverage and provides a lower limit to the sensitivity utilized in this work (we neglect in the present estimates the small increase of this degradation factor with respect to the value $\sqrt{2}$ introduced by the limited sky regions observed during the mission). The estimate of the PLANCK best sensitivity for moving sources assumes to be possible to properly use and to average the information from all the receivers of a specific frequency channel. Of course, a realistic situation may be less favorable, because of the motion of the considered object.

The LFI beams for each channel are located in a ring with a radius of about 4° , on the PLANCK telescope field of view, around the line of sight. The HFI beams are located closer to the center and they may be also at few degrees from the telescope line of sight. On the PLANCK telescope field of view, two coordinates U,V are typically used to identify the beam positions. The direction in the sky of the coordinate V is parallel to the scan circle of the PLANCK telescope line of sight, generated by the spacecraft rotation around its spin axis. The direction in the sky of the coordinate U, orthogonal to V, is, at least for simple scanning strategies (i.e., with the spacecraft spin axis always parallel to the antisolar direction), parallel to the spin axis shift direction during the mission.

Given the spread of the PLANCK LFI beams on the telescope field of view,

another degradation factor, $\sqrt{N_{ric,sky}}$, where $N_{ric,sky}$, ranging from 2 to 16, is the number of radiometers per channel pointing at the same sky position at the same time, has to be taken into account. In column 3 of Table 1 we report the number of LFI radiometers (all intrinsically sensitive to the polarization) and of the unpolarized and polarized HFI bolometers. In the case of the LFI channels the total temperature measurement is given by adding the signals from the two radiometers coupled to a specific feed horn (or beam); therefore, $N_{ric,sky} = N_{rad}/2 = N_{feed}$. In all the cases, except for one feed at 44 GHz, a pair of LFI feeds look at the same scan circle in the sky, being located in the focal plane unit to follow the sky scan direction as the spacecraft spins (each LFI beam, except one at 44 GHz, is symmetrically located to another LFI beam with respect to the axis $V=0$, i.e. they have the same U coordinate). The factor, $\sqrt{N_{ric,sky}}$, reported in Table 2 at 44 GHz, provides a pessimistic value for our sensitivity estimates. A different factor, for most of the cases, and reported in Table 2 for the 30, 70 and 100 GHz channels, is $\sqrt{N_{ric,sky}/2}$. Puget et al. (1998) obtained the sensitivity on temperature fluctuation measurements by combining both unpolarized and polarized detectors for the HFI channels at 143 and 217 GHz. At 545 GHz only polarized detectors will operate, whereas at 100, 353 and 857 GHz only unpolarized detectors are planned. The HFI Focal Plane Unit arrangement is more complex than for LFI and it will be re-defined in few months (B. Maffei, private communication at the PLANCK Systematic Effect Working Group meeting, ESTEC, June 2001). To

Table 2

Instrumental noise estimates for moving sources. The values reported in the columns 2 and 3 refer to the PLANCK sensitivity for moving sources at middle ecliptic latitudes. In the case of low ecliptic latitude objects, we report also the 1σ overall confusion noise including CMB and astrophysical fluctuations, neglecting the information from future space missions (column 4), by considering the information provided by the MAP survey (column 5), and, finally, the sensitivity appropriate to a PLANCK single sky coverage (see also the text).

$\nu_{\text{eff}}/\text{GHz}$	$\sigma_{\text{noise}}/\mu\text{K}$	$\sigma_{\text{noise}}/\text{mJy}$	$\sigma_{\text{overall}}/\text{mJy}$	$\sigma_{\text{after MAP}}/\text{mJy}$	$\sigma_{\text{after Planck}}/\text{mJy}$
30	7–26	19–70	272–283	53–94	29–83
44	11–76	29–153	249–303	77–189	44–178
70	15–62	40–165	228–293	112–215	61–194
100	18–102	47–266	201–362	138–331	72–309
100	4.1–14.7	9.5–34	193–197	127–133	16–41
143	4.8–14.9	16.3–51	151–161	151–161	25–61
217	4.4–11.3	16.3–42	86–97	86–97	25–51
353	3.4–8.3	27.4–67	49–86	49–86	42–82
545	2.8–6.9	53.7–132	108–175	108–175	82–161
857	1.3–3.1	60.8–149	197–252	197–252	93–182

translate the sky map temperature sensitivity of Table 1 to the simple estimate of upper limits for moving sources quoted in Table 2 we consider that analogously to the case of the LFI, the HFI feeds at each frequency are aligned

in two or three groups. The feeds of each group, looking at the same scan circle in the sky, have a very similar value of U . In the case of the PLANCK HFI, we have to include a further degradation factor in the range from $\simeq \sqrt{2}$ to $\simeq \sqrt{3}$. In the sensitivity estimates reported in Table 2 we conservatively use the value $\sqrt{3}$.

A last degradation factor $\sim \sqrt{\text{FWHM}/\Delta\theta_s}$, where $\Delta\theta_s$ (2.5 arcmin) is the spin axis shift between two consecutive hours, takes into account the possibility that a moving object falls out of the beam after a spin axis repointing. This factor has to be applied both to LFI and HFI.

Taking into account all these sensitivity degradation factors, the nominal PLANCK sensitivities can be resumed in the ranges reported in column 2 and 3 of Table 2; we provide these sensitivities in terms of antenna temperature and flux.

In practice, we have to keep in mind that the interesting moving objects are generally located close to the ecliptic plane, where the PLANCK sensitivity is $\simeq 1.15$ worst than the averaged sensitivity. Therefore, the values reported in columns 2 and 3 of Table 2 have to be typically multiplied by $\simeq 1.15$. By taking this factor into account, we report also in Table 2 the sum in quadrature of the PLANCK sensitivity for moving objects as quoted in column 3 and of the astrophysical and cosmological confusion noise sources of Table 1 (column 4), the sum in quadrature of the PLANCK sensitivity for moving objects as quoted in column 3 and of the sensitivity of MAP final maps (column 5) and, finally, the sum in quadrature of the PLANCK sensitivity to moving objects as

quoted in column 3 and of the PLANCK sensitivity appropriate to half mission (column 6). These numbers are indicative because of the large variations of the Galaxy intensity in the sky and the uncertainty of extragalactic source fluctuations at $\nu \gtrsim 143$ GHz (intermediate values are adopted in this work). An important point is represented by the opportunity to combine the millimetric observations of asteroids performed by PLANCK with other data obtained in the same period and in different spectral regions, using ground-based telescopes.

The PLANCK asteroid observation at different frequencies will be obtained within \sim few days, because of the angular size of PLANCK receiver array and the spin axis repointing of 1° per day. Then we may predict to observe an asteroid with PLANCK within a week.

PLANCK will be injected in its Lissajous orbit around L2 after about 3–4 months from the launch and the PLANCK nominal scanning strategy will be certainly decided at least many months before the launch. The effective PLANCK scanning strategy may be slightly different from the nominal one and will be accurately reconstructed in few days from the telemetry data. These requirements will allow to organize an observing campaign, of the objects detected by PLANCK, on ground-based telescopes several months in advance.

The first rough estimate of the flux for an asteroid observed by PLANCK will be delivered in a few days, waiting for a longer period for a more accurate value, at least 6 months corresponding to the survey duration. This estimate should allow a first comparison with the ground-based observations.

3 Threshold detection for asteroids

In the radio range the mean equilibrium temperature T_{eq} of an asteroid, averaged over its extent, is given by:

$$T_{eq} = f(1 - p)^{1/4} r^{-1/2}, \quad (4)$$

where p is the bolometric albedo and r the heliocentric distance. In the non-rotating case f is 329, and for our fast rotating asteroids (few hours) f is 277. For instance in the case of 1 Ceres, the mean distance from the Sun is 2.767 AU and the albedo is 0.06 (Morrison 1974), which give an equilibrium temperature of 165 K.

The asteroid equilibrium temperature is related to the asteroid antenna temperature, both averaged over the asteroid extent, by:

$$T_{\nu,ant,obj}^* = e_\nu T_{eq}, \quad (5)$$

with e_ν the emissivity of the asteroid at the frequency ν . In this work we need to define a mean value of $T_{\nu,ant,obj}^*$ for the main belt asteroids in order to determine the threshold detection. We will assume the emissivity close to unity, since we are considering objects with $T_{eq} \approx 100$ K and working at millimetric wavelengths.

The antenna temperature observed at a specific frequency ν is given by the convolution, over the whole solid angle, of the antenna temperature, of the

considered asteroid, with the antenna beam pattern response (we assume the antenna responses normalized to the maximum, i.e. $J = 1$ at the beam center direction):

$$T_{\nu,ant,obs}(t) = \frac{\int_{4\pi} T_{\nu,ant,obj}(\hat{\gamma}, t) J(\hat{\gamma}, t) d\Omega}{\int_{4\pi} J(\hat{\gamma}) d\Omega}; \quad (6)$$

in this equation $\hat{\gamma}$ is a unit vector identifying a generic direction in the sky. As evident from this equation, the observed antenna temperature depends on the considered observation time because of the spacecraft rotation and scanning strategy and the variation of the asteroid properties. Note that, at least in principle, this equation includes possible deviations from the uniformity of the asteroid equilibrium temperature on its surface; since the small angular sizes of the considered objects, they will be neglected in the following, we will work with quantities averaged over the asteroid surface.

The maximum observed antenna temperature will be obtained when the antenna beam center points at the asteroid center. By assuming a bi-dimensional perfectly symmetric Gaussian beam shape and in the limit of asteroid angular sizes much smaller than the beam FWHM, the maximum observed antenna temperature can be approximated by the expression:

$$T_{\nu,ant,obs}^{max} \simeq 4\ln 2 T_{\nu,ant,obj}^* \frac{[R/d]^2}{(\text{FWHM}/\text{rad})^2}, \quad (7)$$

where $T_{\nu,ant,obj}^* \simeq T_{eq}$ ($e_\nu \simeq 1$), given by $T_{\nu,ant,obj}^* = \int_{4\pi} T_{\nu,ant,obj}(\hat{\gamma}, t) d\Omega / \Omega_{obj}$, is the average over the object extent of the object antenna temperature and

$\Omega_{obj} = \pi[R/d]^2$ is the solid angle subtended by the object, d being its distance from the spacecraft and R its effective radius at the considered observation time.

Assuming 150K as mean value of the asteroid antenna temperature, a geocentric distance range between 2 and 4 AU (1.5×10^8 km) and a radius range between 50 and 500 km, we obtain R/d in the range:

$$R/d \sim 2 \times 10^{-7} - 2 \times 10^{-6}. \quad (8)$$

These values can be converted in the maximum antenna temperature, for a specific frequency and beam FWHM, using equation (7):

$$T_{\nu,ant,obs}^{max} \simeq (0.2 - 20)\text{mK} \frac{1}{(\text{FWHM}/\text{arcmin})^2}. \quad (9)$$

The antenna temperature range for some PLANCK channels is:

$$30\text{GHz} , \text{ FWHM} \simeq 33' \rightarrow T_{\nu,ant,obs}^{max} \simeq (0.2 - 20)\mu\text{K} \quad (10)$$

$$100\text{GHz} , \text{ FWHM} \simeq 10' \rightarrow T_{\nu,ant,obs}^{max} \simeq (2 - 200)\mu\text{K} \quad (11)$$

$$217 - 550\text{GHz} , \text{ FWHM} \simeq 5' \rightarrow T_{\nu,ant,obs}^{max} \simeq (10 - 1000)\mu\text{K}. \quad (12)$$

Comparing these values with the noise reported in table 2 we can see that, mainly at the HFI frequencies, there are good chances to observe asteroids and for higher R/d even with the LFI channels.

In the numerical model we consider only asteroids with R/d larger than 10^{-7}

(a value referred as “threshold” in the following), since for smaller R/d the maximum signal is less than about $1\sigma_{\text{noise}}$ quoted in Table 2 also for the most favorable channels, and there is then no realistic chance to derive information on their properties⁴ (on the contrary, values of R/d smaller than this threshold have to be considered in the cleaning of PLANCK data streams from asteroid contamination).

4 Identification of target asteroids in the Planck field of view

4.1 The numerical algorithm

To estimate the number of asteroids that will be seen by the LFI and HFI channels during the PLANCK survey and the precise dates of observation we have developed a numerical code that calculates the orbits of all large asteroids and checks if they fall within the resolution element of a beam. The initial orbital elements of all asteroids larger than 50 km are taken from a datafile provided by Bowell (2000) while the orbits of the nine planets are derived from the JPL ephemerides at the corresponding epoch. The diameters are known for most asteroids larger than 50 km and are reported in Bowell’s file. For

⁴ It can be noted that, since the CMB fluctuations dominate the sky confusion noise between ~ 50 and ~ 250 GHz, combining more frequency channels decreases the 1σ overall confusion noise quoted for each frequency channel in the last column of Table 2.

those asteroids whose diameter is not reported in Bowell’s file, we used the value given in the file of 12,487 asteroids adopted by Zappalá et al. (1995) for asteroid family search. Whenever the albedo is not directly known from observations, an average value, typical of that particular zone of the asteroid belt, is used to derive the diameter of the body. To compute the orbits of the asteroids and planets we have adopted the RA15 version of the numerical integrator RADAU (Everhart 1985) with the highest value of the precision parameter.

At the end of every timestep, we compute the position of each asteroid respect to the Earth since the PLANCK surveyor will orbit together with the Earth at its L2 Lagrangian point. Since we know from the mission specifications the direction of each beam, we can easily calculate the angle between the asteroid and the antisolar direction and the center of the beam of each LFI and HFI channel. A possible future refining will be to compute at each epoch the position of the spacecraft and compute directly the angle of the asteroid with respect to the spacecraft. We fixed the timestep of the numerical integration to 1 hr, that is the time required by all the channels to complete a 360° scan. Thanks to this choice we can directly compare the position of the asteroid with all the channel beam directions during the scan at once. A detection is signalled whenever the angle between the asteroid and the antisolar direction is within the direction of the beam divided $+/-$ the $\text{FWHM}/2$.

The input data for the code, apart from the orbital parameters, are the angles that define the inclination of each beam respect to the antisolar direction. The

code begins the comparison between the position of the asteroids and that of the beam at the nominal start of the mission and it continues for two years. The code at the end of the run will give the list of those asteroids that will be observed by each horn, with the relative date of observation and R/d ratio. The output include also a list, for each channel, of the dates when an asteroid will be present in the field of view of the beam during the scan.

4.2 Results

At the end of the simulation 397 asteroids were observed during the nominal length of the mission in at least one of the horns of PLANCK with a R/d high enough for individual detection. For a significant fraction of them (in the range from ~ 50 to 100 objects) the good S/N ratio will allow to determine the antenna temperature and information on the physical properties of the asteroid's regolith. The determination of the antenna temperature at different frequencies may be useful to derive models for the surface layers and establish some bounds on the depth of the surface layer and the dielectric properties of the material.

The times (i.e. the different consecutive scan circles) an asteroid is consecutively observed by the same horn during a single passage ranges from 3 to 6 depending on the FWHM of the channel. It means that on average an asteroid passage lasts about 3–6 hours. In some cases more horns, belonging to the same frequency channel, may be crossed within some hours allowing to deter-

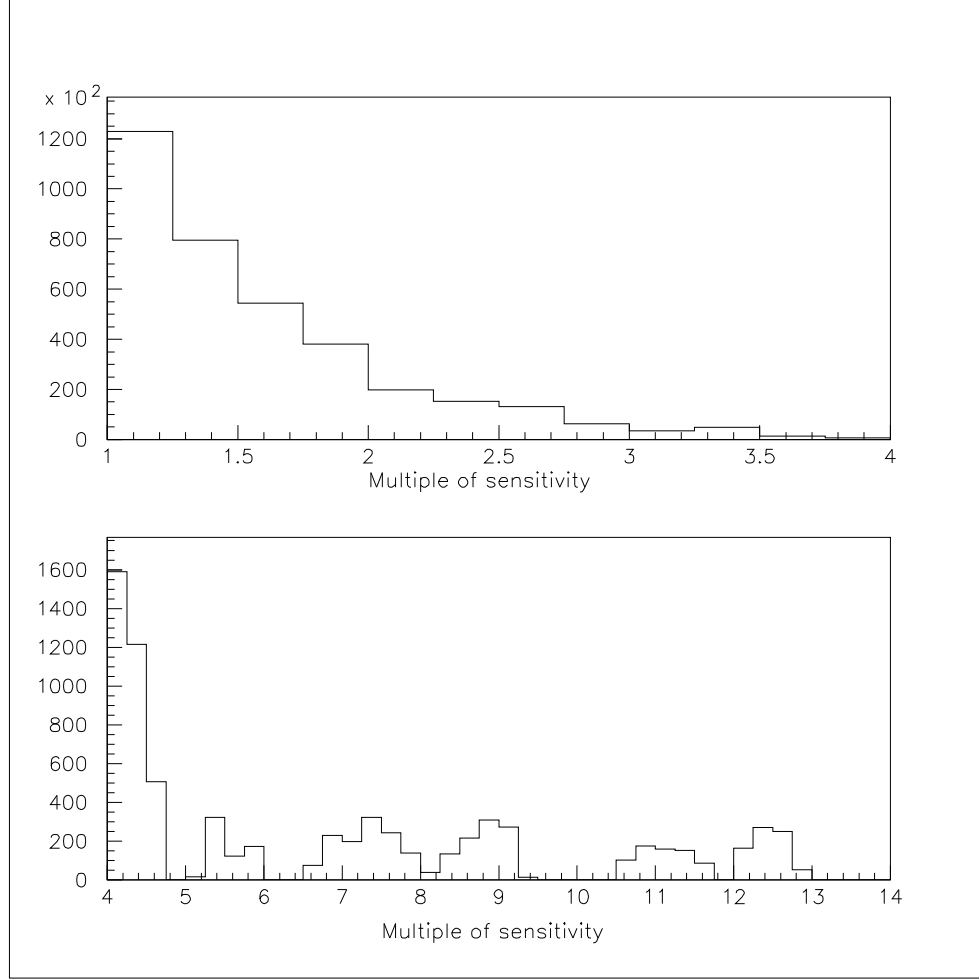
mine a radio light-curve. In other cases, horns of different frequencies may be crossed allowing to get information on the thermal emission of the asteroid. From a statistical point of view, asteroids will be observed by each channel of both LFI and HFI in 30% of the total scan circles performed in the mission. This datum must be taken into account in the extraction of the Galactic and extragalactic radio sources from PLANCK time ordinary data.

In Fig.2 the histograms shows the intensity of the signal at detection as multiple of the minimum detection threshold $R/d \sim 10^{-7}$ for all the observed asteroids on all channels. For large asteroids the radio signal as detected by the PLANCK horns reaches values as large as 12 times the detection threshold. In the plot at the bottom of Fig. 2 we may notice the signals from the 5 largest asteroids and, so on at smaller R/d ratio, from all the other visible objects. Of course, the number of detected asteroids increases drastically if the sensitivity threshold is reduced since the asteroid size distribution is a power law. In Table 3 we report the cumulative and differential number of asteroids detectable at different levels of the R/d ratio.

5 Conclusions

The PLANCK ESA mission will perform a high-angular resolution mapping of the microwave sky over a wide range of frequencies, from 30 to 900 GHz. During the two years planned for the mission the surveyor will frame a large

Fig. 1. Number of observations of asteroids by PLANCK, during the whole mission at different sensitivity levels ($\times 10^{-7}$). In the bottom plot at high signal intensity only the 5 largest asteroids appear in PLANCK's horns. The increasing number of small asteroids that can be observed at lower sensitivity explains the growing amount of detections.



number of main-belt asteroids. In this paper we investigate in detail for the first time the possibility for PLANCK to detect main-belt asteroids. The main parameter in the asteroid detection process by the PLANCK horns is the R/d ratio. The instrumental sensitivity to such objects has then been defined as the minimum R/d value required to safely observe them. This value is given

Table 3

Cumulative and differential number of asteroids may be detected at different R/d values.

R/d	Differential number	Cumulative number
$1-2 \times 10^{-7}$	299	397
$2-3 \times 10^{-7}$	76	98
$3-4 \times 10^{-7}$	15	22
$4-5 \times 10^{-7}$	4	7
$5-6 \times 10^{-7}$	0	3
$6-7 \times 10^{-7}$	0	3
$7-8 \times 10^{-7}$	0	3
$8-9 \times 10^{-7}$	1	3
$9-10 \times 10^{-7}$	1	2
$1-2 \times 10^{-6}$	0	1
$2-3 \times 10^{-6}$	0	1
$3-4 \times 10^{-6}$	1	1

by the PLANCK sensitivity at different frequencies rescaled to take into account the integration time and the confusion noise due to the background. An accurate evaluation of the noises and the sensitivity degradation, related to the high proper motion of the asteroids, yielded a minimum R/d ratio of $(R/d)_{\min} \sim 10^{-7}$.

A numerical simulation of a two-years mission has been performed in order to estimate the number of objects whose (R/d) is greater than about 10^{-7} and that will then be observed by PLANCK. The simulation uses updated catalogs for the orbital elements of the main-belt asteroids and their diameters. The orbit of each asteroid has been integrated with a very short timestep to compute the relative position of the body with respect to the PLANCK horns and the value of (R/d) . An accurate mission simulation has been obtained.

Up to 397 asteroids are expected to be detected in the various PLANCK channels (Table 3). Detectable asteroids will appear in about 30% of the total sky circles scanned by the mission.

The previous survey of Main Belt Asteroids was performed by the Infrared Astronomical Satellite (IRAS) on 1983 in four wavelength bands centered near 12, 25, 60 and $100\mu\text{m}$, much lower than the minimum wavelength observed by PLANCK of $350\mu\text{m}$, corresponding to the highest frequency of 857 GHz. It surveyed approximately 96% of the sky and 2228 different multiply observed asteroids were associated to IRAS sources (Tedesco et al. 2002), providing a good estimate of diameter and albedo for most of them.

IRAS's $12\mu\text{m}$ limiting sensitivity, for $\text{S}/\text{N}=3$, was about 150 mJy (Tedesco and Desert 2002), and assuming a Main Belt Asteroid as a black body at 150 K this flux can be translated to about 56 mJy at $350\mu\text{m}$ (857 GHz), well below the PLANCK noises reported in Table 2.

PLANCK will provide flux measurements for a smaller sample of asteroids ($\sim 50 - 100$ objects) compared to IRAS, but at different wavelengths, almost unexplored for this class of Solar System objects. This will improve our understanding of the thermal emission and the related surface properties of asteroids.

6 Acknowledgements

It is a pleasure to thank M. Bersanelli, C.R. Butler, K. Ganga, D. Maino, N. Mandolesi, F. Pasian, M. Sandri, F. Villa for useful discussions on PLANCK performances and simulations, and L. Danese, G. De Zotti, L. Terenzi, L. Toffolatti, N. Vittorio for helpful conversations on astrophysical and cosmological confusion noise. We thank the LFI Consortium for having promptly provided us with the updated LFI beam positions and sensitivities.

References

Altenhoff, W.J., Johnston, K.J., Stumpff, P., & Webster, W.J., 1994, A&A, 287, 641.

Bowell, T., June 2000, ftp.lowell.edu

Burigana, C. 2000, Int. Rep. ITeSRE/CNR 298/2000, October

Burigana, C. 2001, Int. Rep. ITeSRE/CNR 322/2001, August

De Zotti, G., Toffolatti, L., Argüeso Gómez, F., et al 1999a, Proceedings of the ECTMR Conference 3 K Cosmology, Roma, Italy, 5-10 October 1998, AIP Conference Proc. 476, ed. Maiani L., Melchiorri F., & Vittorio N., 204, astro-ph/9902103

De Zotti, G., Gruppioni, C., Ciliegi, P., Burigana, C., & Danese, L. 1999b, New Astron., 4, 481

Delabrouille, J. 1998, A&AS, 127, 555

Everhart E., 1985, *Astrop.Space Sci.*, 115, 185

Janssen, M., Scott, D., White, M., et al. 1996, [[astro-ph/9602009](#)]

Magliocchetti, M., Moscardini, L., Panuzzo, P., et al. 2001, *MNRAS*, in press,

[[astro-ph/0102464](#)]

Maino, D., Burigana, C., Górski, K.M., Mandolesi, N., Bersanelli, M. 2001, *A&A*, submitted

Mandolesi, N., et al. 1998, *PLANCK Low Frequency Instrument, A Proposal Submitted to ESA*

Mather, J.C., Fixsen, D.J., Shafer, R.A., Mosier, C., & Wilkinson, D.T. 1999, *ApJ*, 512, 511

Morrison, D.D., 1974, *ApJ*, 194, 203.

Neufeld, D.A., Stauffer, J.R., Bergin, E.A., et al. 2000, *ApJ*, 539, L151.

Puget, J.L., et al. 1998, *High Frequency Instrument for the PLANCK Mission, A Proposal Submitted to the ESA*

Redman, R.O., Feldman, P.A., & Matthews, H.E., 1998, *AJ*, 116, 1478.

Redman, R.O., Feldman, P.A., Matthews, H.E., Halliday, I., Creutzberg, F., 1992, *AJ*, 104, 405.

Sandri, M., and Villa, F., July 2001, PL-LFI-PST-TN-027, private reference

Stanghellini, G., Burigana, C., Maino, D., et al. 2001, *Int. Rep. ITeSRE/CNR* 310/2001, March

Tedesco, E.F., Noah, P.V., Noah, M., Price, S.D., 2002, AJ, 123, 1056.

Tedesco, E.F., Desert, F.-X., 2002, AJ, 123, 2070.

Toffolatti, L., Argüeso Gómez, F., De Zotti, G., et al 1998, MNRAS, 297, 117

Zappalá, V., Bendjoya, Ph., Cellino, A., Farinella, P., Froeschle, C., 1995, Icarus, 116, 291